**Supporting Material**

# Ion-controlled conformational dynamics in the outward-open transition from an occluded state of LeuT

Chunfeng Zhao, Sebastian Stolzenberg, Luis Gracia, Harel Weinstein, Sergei Noskov, Lei Shi

## SUPPORTING METHODS

**Computation of $Na^+/K^+$ and $Na^+/Li^+$ selectivity.** Ion selectivity of the single monovalent $Na^+$ binding site was computed with the equation:

$$\Delta\Delta G_{Na^+\to X^+} = \Delta G^{site}_{Na^+\to X^+} - \Delta G^{bulk}_{Na^+\to X^+}$$

where X is either K or Li. $\Delta G^{site}_{Na^+\to X^+}$ is the relative free energy of perturbing $Na^+$ to $X^+$ at the ion binding site, and $\Delta G^{bulk}_{Na^+\to X^+}$ is the relative free energy of perturbing $Na^+$ to $X^+$ in bulk water (1). These relative binding free energies were computed using free energy perturbation/molecular dynamics (FEP/MD) simulations (2). Based on the results from our PCA analysis, we chose eight frames along the transition path (PC1) from the occluded to the outward-open conformation, labeled as F1-F8, for evaluation of the selectivity. For each frame, the structure was reinitialized (the velocities of the atoms are reassigned so that the entire system is set to 310 K) and equilibrated for 200 ps using the CHARMM program (3), version c36a2. The same parameter (4) and equivalent protein structure files as those in the equilibrium MD with NAMD have been used throughout in the FEP/MD with CHARMM. To ensure that the coordination to Na1 is maintained throughout the CHARMM equilibration, a BESTFIT RMSD harmonic restraint was applied to the Na1 site for the first 100 ps of equilibration. Then the restraint was removed, and unconstrained equilibration was carried out for the next 100 ps. Pressure and temperature were kept constant (1 atm and 310 K, respectively). Periodic boundary conditions were used for the orthorhombic system. Electrostatic interactions were treated with a particle mesh Ewald algorithm (5). The relative binding free energy of Na1:Na2 to K1:Na2 and Na1:Na2 to Li1:Na2 were then calculated using the CHARMM PERTurb function. Each FEP experiment was run in windowed mode with 42 windows (21 forward and 21 backward) and 200 ps per window. The integration time step used was set to 1 fs. The thermodynamic coupling parameter ($\lambda$) range was between 0.0 and 1.0 with an increment of 0.05. The weighted histogram analysis (WHAM) method was then used to post-process the FEP data (6). The mean and standard deviations were computed after blocking the data into 16 blocks determined with the block average protocol for error analysis of molecular simulations (7). For all the frames, the forward and backward free energies of perturbation are within 1 kcal/mol and the average values are reported. To compute $\Delta G^{bulk}_{Na^+\to X^+}$, similar FEP/MD simulations were carried out for the system of $Na^+$ solvated in 1125 water molecules. The values obtained for bulk hydration free energy differences, 18.49 kcal/mol for $\Delta G^{bulk}_{Na^+\to K^+}$, and -22.84 kcal/mol for $\Delta G^{bulk}_{Na^+\to Li^+}$, were used for computations of the selectivity free energies for frames F1-F8 described above.

**Alchemical transformation to annihilate Na1 and to protonate Glu290.** It is difficult for classic MD to overcome the energy barriers associated with alchemical transformation in a short simulation time. FEP/MD divides an alchemical process ($\lambda$: 0->1) into many perturbation steps with smaller energy barriers. Although small, these incremental changes are expected to overcome the energy barriers efficiently in producing the necessary conformational rearrangements. Since neither the scale nor the scheme of the energy barriers is known beforehand, it becomes necessary to adjust the step size for a particular transformation to keep the free energy change ($\Delta G$) for each FEP step sufficiently small. Doing this manually is impractical and therefore we developed an automated FEP/MD protocol for NAMD. In this protocol, we proceed to a next step after a step ($\lambda_a$->$\lambda_b$), if and only if $|\Delta G_{\lambda a\to\lambda b}| < \Delta G_{max} \equiv 4kT$; in the next step $\lambda_b$ -> $\lambda_c$, the $\lambda_c$ satisfies: $\Delta G_{ideal}/(\lambda_c-\lambda_b)=|\Delta G_{\lambda a\to\lambda b}|/(\lambda_b-\lambda_a)$, so that $|\Delta G_{\lambda b\to\lambda c}|$ is projected to be $\sim\Delta G_{ideal} \equiv 2kT$. In this manner, $\lambda_c \equiv \lambda_b+(\lambda_b-\lambda_a)*r$, where $r \equiv \min(\Delta G_{ideal}/|\Delta G_{\lambda a\to\lambda b}|,$

$r_{max}$), and $r_{max} \equiv 2$ ensures that $\lambda$ does change drastically. But if in the step ($\lambda_a \rightarrow \lambda_b$) the $|\Delta G_{\lambda a \rightarrow \lambda b}| \geq \Delta G_{max}$, we re-do the perturbation from $\lambda_a$ to $\lambda_{b'} \equiv \lambda_a + (\lambda_b - \lambda_a)*r$ so as to have $\lambda_{b'}$ satisfy $\Delta G_{ideal}/(\lambda_{b'} - \lambda_a) = |\Delta G_{\lambda b \rightarrow \lambda a}|/(\lambda_b - \lambda_a)$ as above. Again, we proceed, if and only if $|\Delta G_{\lambda a \rightarrow \lambda b'}| < \Delta G_{max}$, etc. In our simulations, each step was 100 ps long, including an equilibration phase of 5 ps. The steps at the start and end were chosen to be small ($\lambda$=0,1e-5,3e-5,7e-5,1.5e-4 and $\lambda$=0.99,0.999, 0.9999,0.99999,0.999999,1,1) to help avoid the potential "end-point catastrophe". We applied this FEP protocol on the snapshots at 60 ns and 720 ns of the MD1 trajectory to annihilate Na1 first (with 117 and 115 steps taken, respectively), while a bulk water molecule was simultaneously transformed into a $Na^+$ ion to maintain the neutral charge of the system; also with this protocol, Glu290 was protonated using the dual-topology scheme (with 112 and 110 steps taken, respectively), while a bulk $Na^+$ ion was simultaneously transformed into water. In total, four MD simulations were carried out from the end points of both steps of transformations (see text).

**Figure S1.** Comparison of fitting schemes. (*A*) The $C_\alpha$-RMSF against residue index for three different RMSD fitting schemes: the iterative fitting on all $C_\alpha$ atoms ("iterative fitting", red), and the standard RMSD fitting based on either all $C_\alpha$ atoms ("all $C_\alpha$", blue) or the $C_\alpha$ atoms of the transmembrane (TM) domain and EL4 ("all TM-EL4 $C_\alpha$", green), which is derived from our understanding of membrane proteins that the structured TM regions are more stable. . All three RMSF curves have similar patterns. (*B*) Differences in RMSF (ΔRMSF), i.e., "iterative fitting"-"all $C_\alpha$" (red), "all-TM and EL4 $C_\alpha$"-"all $C_\alpha$" (green). Note that both "iterative fit" and "all-TM and EL4 $C_\alpha$" tend to have larger RMSF values for the flexible loop regions and smaller ones for the stable TM regions, than the non-biased "all $C_\alpha$" scheme. (*C*) The "iterative fitting" weights (red lines) show good agreement with the TM and EL4 regions (green bars) used for the "all-TM and EL4 $C_\alpha$" scheme.

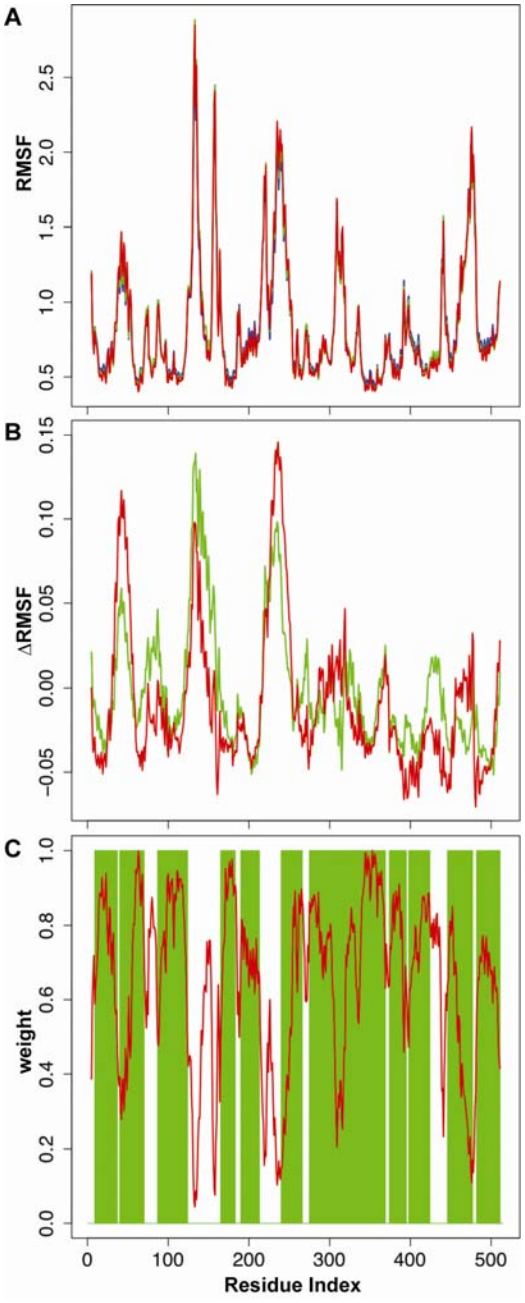

**Figure S2.** Analysis of the conformational transition in the MD2. The time-dependent evolution of $C_\alpha$-iRMSD$_{2A65}$ and $C_\alpha$-iRMSD$_{3F3A}$ (*A*), water molecules in the extracellular vestibule (*B*), and the mapping of $\gamma_1(t)$ on the $C_\alpha$-iRMSD$_{2A65}$ vs. $C_\alpha$-iRMSD$_{3F3A}$ plot (*C*) are presented as those for MD1 in Fig. 1.

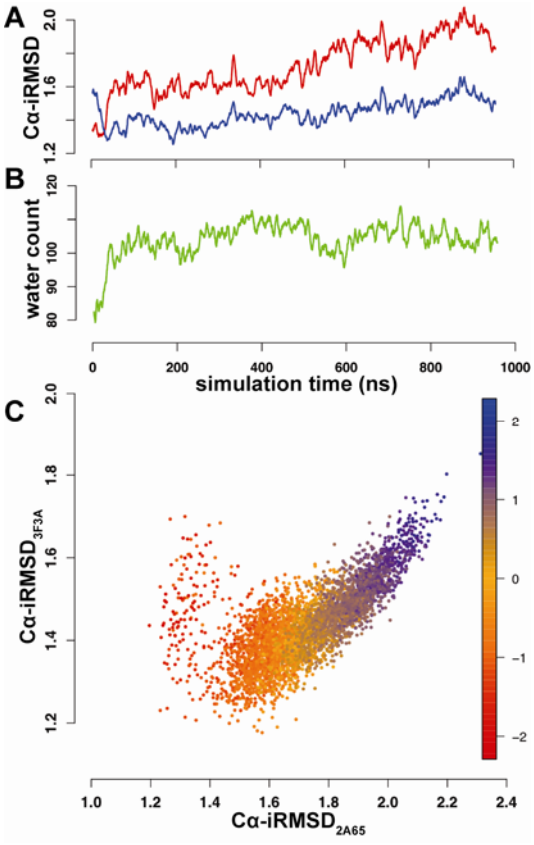

**Figure S3.** Pearson Correlation analysis among various observables along the MD1 trajectory. The observables include i) the Na1 and Na2 enthalpies, ii) iRMSD, iii) trajectory overlaps for PC1 to PC3, iv) the top 5 correlated HA/HD for each column in Table S3, v) the distances to Na1, and vi) the numbers of waters surrounding Na1. Note the top HAs and HDs correlated with the Na2 affinity are less correlated than those for the Na1 affinity and PC1.

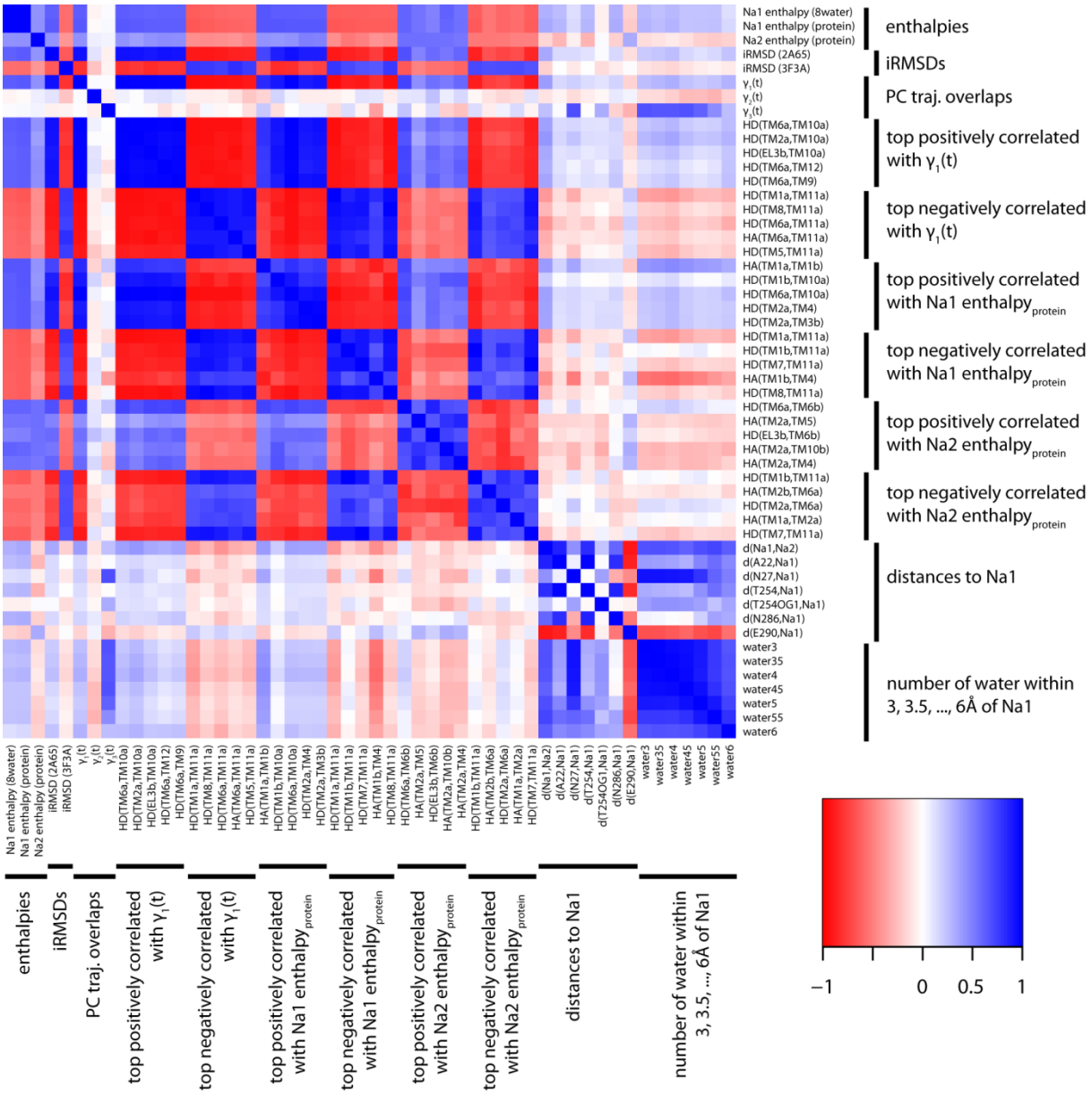

**Figure S4.** Trajectories of the umbrella sampling simulations for the outward-open 3F3A-like frame F8 of LeuT. The trajectories for the 109 umbrella sampling windows centered from z(Na1) = -2.5Å to z(Na1) = 24.5Å were oriented to the starting structure. The Na1 positions, 49 frames for each window, are then shown as small spheres. Na1 is colored as blue, red, grey, orange, yellow, tan, silver, green, white, pink, and purple for the umbrella sampling windows centered at [-2.50, -0.25], [0.00,2.25], [2.50,4.75], [5.00,7.25], [7.50,9.75], [10.00,12.25], [12.50,14.75], [15.00,17.25], [17.50,19.75], [20.00,22.25], and [22.50,24.50] respectively. The protein is represented as a cartoon in the left panel, while residues forming the Na1 and the Na1' sites, several residues in the extracellular vestibule (Glu470, Arg30, and Asp404), and Na2 ion are shown in various representations in the right panel. The Na1 site is occupied by a cluster of blue and red spheres, while the Na1' site is occupied by a cluster of red and grey spheres. These trajectories indicate that negatively charged residues Glu470 and Asp404 may play important roles in attracting $Na^+$ from extracellular milieu. After passing through the broken extracellular thin gate (Arg30-Asp404), $Na^+$ is likely facilitated by the negatively charged Glu290 to reach the Na1 site. The arrows indicate potential routes of $Na^+$ entry.

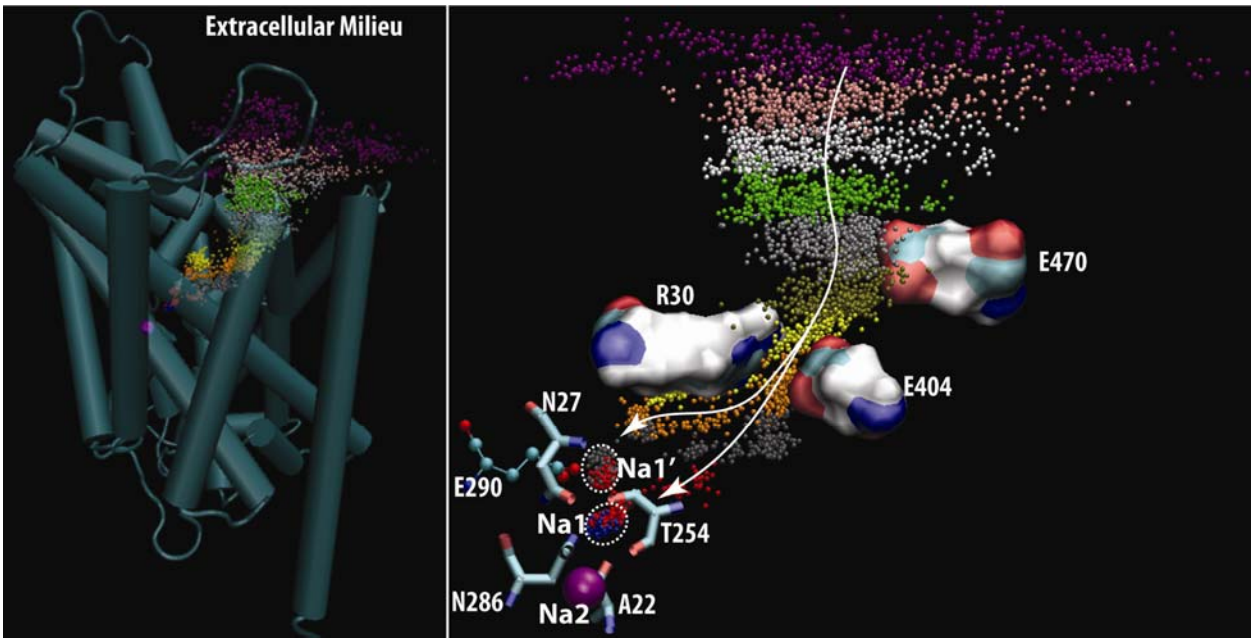

**Figure S5.** The zoom-in views of Fig. 5B for the selected periods.

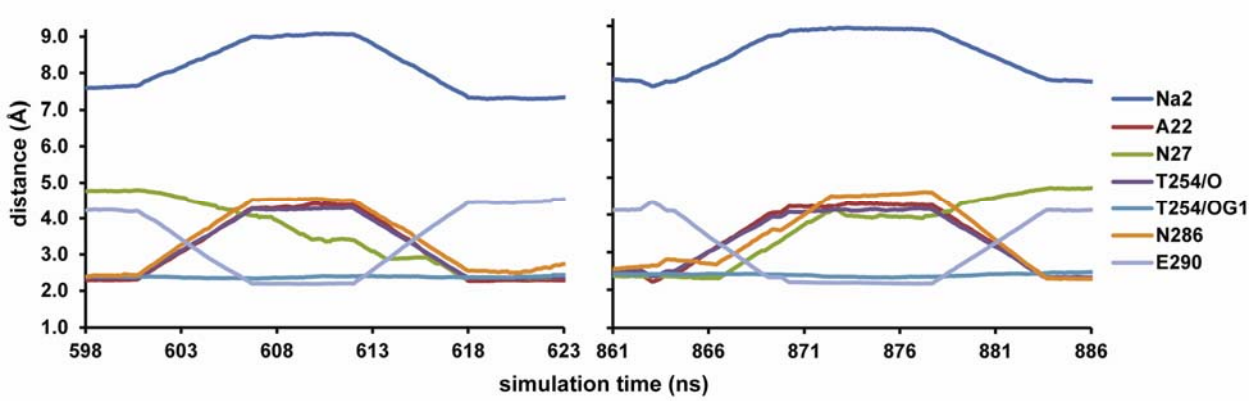

**Figure S6. The protonation of Glu290 in the absence of Na1 has a dehydration effect on the Na1 site vicinity.** The evolutions of the distance of the closest water (oxygen atom) to the side chain of Glu290 are shown for four no-Na1 trajectories. The protonated Glu290 rarely has direct contact with water molecules, especially when the simulation is started from a more occluded state (left panel, see text), in which the closest water can be as far as 8 Å away. The plots are moving averages of 6 ns.

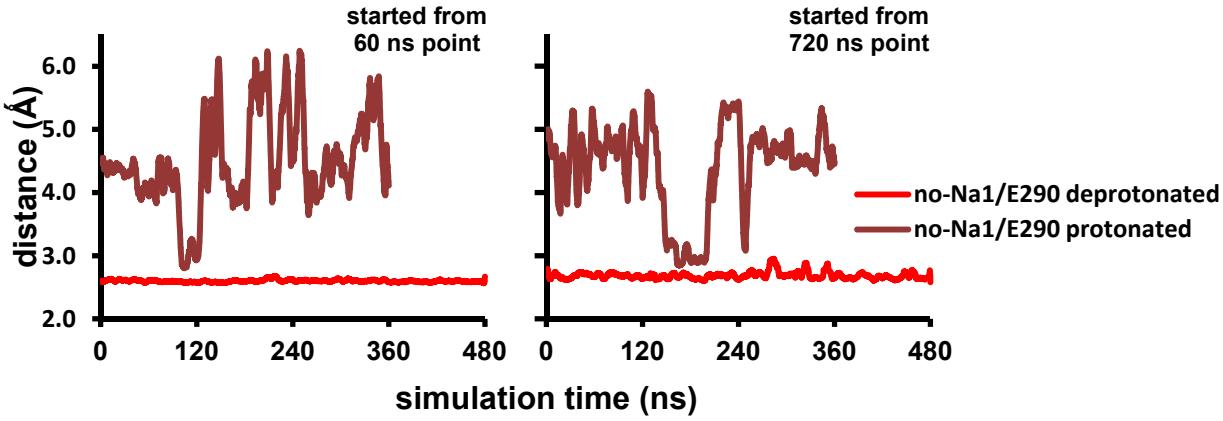

**Table S1.** PC Properties of the MD trajectories (see methods for the definitions of the properties)**.**

(*A*) MD1

| ***i*** | **Eigen value** | $\kappa_i$ | $\chi_i$ | **acos ($\chi_i$)** |
|---|---|---|---|---|
| 1 | 1.13 | 0.26 | 0.79 | 37.35 |
| 2 | 0.30 | 0.07 | 0.10 | 83.98 |
| 3 | 0.26 | 0.06 | 0.13 | 82.73 |
| 4 | 0.20 | 0.05 | 0.31 | 71.76 |
| 5 | 0.15 | 0.03 | 0.00 | 90.00 |
| 6 | 0.14 | 0.03 | 0.11 | 83.45 |
| 7 | 0.11 | 0.03 | 0.06 | 86.37 |
| 8 | 0.10 | 0.02 | 0.29 | 72.85 |

(*B*) MD2

| ***i*** | **Eigen value** | $\kappa_i$ | $\chi_i$ | **acos ($\chi_i$)** |
|---|---|---|---|---|
| 1 | 0.80 | 0.21 | 0.16 | 80.72 |
| 2 | 0.25 | 0.07 | 0.57 | 55.06 |
| 3 | 0.18 | 0.05 | 0.54 | 57.54 |
| 4 | 0.15 | 0.04 | 0.00 | 90.00 |
| 5 | 0.13 | 0.03 | 0.17 | 80.37 |
| 6 | 0.11 | 0.03 | 0.06 | 86.37 |
| 7 | 0.11 | 0.03 | 0.18 | 79.86 |
| 8 | 0.09 | 0.02 | 0.11 | 83.71 |

**Table S2.** Top positively and negatively correlated HAs and HDs with PC1, Na1 enthalpy$_{protein}$, and Na2 enthalpy$_{protein}$.

| $\gamma_1$(t) | | | Na1 enthalpy | | | Na2 enthalpy | | |
|---|---|---|---|---|---|---|---|---|
| *Structural element pair* | *type* | *correlation coefficient* | *structural element pair* | *type* | *correlation coefficient* | *structural element pair* | *type* | *correlation coefficient* |
| TM6a-TM10a | HD | 0.99 | **TM1a-TM1b** | HA | 0.66 | TM6a-**TM6b** | HD | 0.56 |
| TM2a-TM10a | HD | 0.98 | **TM1b-TM10a** | **HD** | **0.66** | TM2a-TM5 | HA | 0.56 |
| EL3b-TM10a | HD | 0.98 | **TM6a-TM10a** | **HD** | **0.66** | EL3b-**TM6b** | HD | 0.56 |
| TM6a-TM12 | HD | 0.98 | **TM2a-TM4** | **HD** | **0.66** | **TM2a-TM10b** | **HA** | **0.55** |
| TM6a-TM9 | HD | 0.97 | **TM2a-TM3b** | **HD** | **0.65** | **TM2a-TM4** | **HA** | **0.53** |
| TM3a-TM6a | HD | 0.97 | **TM2a-TM10a** | **HD** | **0.64** | EL3b-TM10b | HD | 0.52 |
| EL3b-TM12 | HD | 0.96 | **TM1b-TM9** | **HD** | **0.63** | EL3b-TM11a | HD | 0.52 |
| EL3b-TM9 | HD | 0.96 | TM2a-TM8 | HD | 0.63 | TM11a-TM11b | HD | 0.52 |
| TM2a-TM9 | HD | 0.96 | TM1b-TM3b | HD | 0.63 | TM2b-EL3b | HD | 0.51 |
| TM2a-TM3a | HD | 0.96 | **TM6a-TM12** | **HD** | **0.63** | TM6a-TM11b | HD | 0.51 |
| TM4-TM6a | HD | 0.96 | **TM6a-TM9** | **HD** | **0.63** | TM1b-TM4 | HD | 0.51 |
| TM3b-TM6a | HD | 0.95 | **EL3b-TM10a** | **HD** | **0.63** | TM2b-TM6a | HD | 0.50 |
| TM2a-TM12 | HD | 0.95 | **EL3a-TM10a** | **HD** | **0.63** | TM1b-TM3b | HD | 0.50 |
| TM6a-TM8 | HD | 0.95 | **TM2a-TM12** | **HA** | **0.63** | **TM2a-TM4** | **HD** | **0.50** |
| TM3a-EL3b | HD | 0.94 | **EL3b-TM12** | **HD** | **0.63** | TM2a-TM11b | HD | 0.49 |
| TM2a-TM10b | HD | 0.93 | **TM2a-TM9** | **HD** | **0.62** | IL2-EL3b | HD | 0.49 |
| EL3a-TM10a | HD | 0.93 | **TM4-TM6a** | **HD** | **0.62** | **TM2a-TM3b** | **HD** | **0.49** |
| EL3b-TM11b | HD | 0.93 | TM1b-TM4 | HD | 0.62 | **TM3a-EL3b** | **HD** | **0.48** |
| TM3b-EL3b | HD | 0.92 | **TM1b-TM11a** | **HA** | **0.61** | TM2a-**TM6b** | HD | 0.47 |
| TM4-EL3b | HD | 0.92 | **TM3b-TM6a** | **HD** | **0.61** | TM2a-TM8 | HD | 0.47 |
| TM2a-TM3b | HD | 0.92 | **TM3a-TM6a** | **HD** | **0.61** | **EL3b-TM12** | **HD** | **0.47** |
| TM6a-TM10b | HD | 0.92 | **TM3a-EL3b** | **HD** | **0.61** | **EL3b-TM11b** | **HD** | **0.47** |
| IL2-TM6a | HD | 0.91 | **TM1b-TM9** | **HA** | **0.61** | **TM6a-TM10b** | **HD** | **0.47** |
| TM3a-EL3a | HD | 0.91 | EL3b-TM10b | HD | 0.61 | **TM2a-TM12** | **HA** | **0.46** |
| TM1b-TM10a | HD | 0.91 | TM6a-**TM6b** | HD | 0.61 | TM6a-EL4b | HA | 0.46 |
| EL3a-TM11a | HA | 0.90 | **TM2a-TM10b** | **HA** | **0.60** | **TM1b-TM9** | **HD** | **0.45** |
| TM2a-IL2 | HD | 0.90 | **TM6a-TM8** | **HD** | **0.60** | **TM6a-TM12** | **HD** | **0.45** |
| TM1b-TM11a | HA | 0.89 | | | | **TM3a-TM6a** | **HD** | **0.45** |
| TM2a-TM4 | HD | 0.89 | | | | **TM4-TM6a** | **HD** | **0.45** |
| TM1b-TM9 | HD | 0.89 | | | | | | |
| common with PC1 positive pairs | | | | | **21/27** | | | **13/29** |
| TM1a-TM11a | HD | -0.95 | **TM1a-TM11a** | **HD** | **-0.66** | **TM1b-TM11a** | **HD** | **-0.53** |
| TM8-TM11a | HD | -0.94 | **TM1b-TM11a** | **HD** | **-0.65** | TM2b-TM6a | HA | -0.53 |
| TM6a-TM11a | HD | -0.94 | **TM7-TM11a** | **HD** | **-0.64** | TM2a-TM6a | HD | -0.52 |
| TM6a-TM11a | HA | -0.92 | TM1b-TM4 | HA | -0.63 | TM1a-TM2a | HA | -0.50 |
| TM5-TM11a | HD | -0.90 | **TM8-TM11a** | **HD** | **-0.63** | **TM7-TM11a** | **HD** | **-0.49** |
| TM7-TM11a | HD | -0.90 | **TM6a-TM11a** | **HD** | **-0.62** | TM2a-TM11a | HA | -0.49 |
| TM3b-TM11a | HD | -0.90 | TM7-TM10b | HA | -0.62 | TM1b-TM7 | HD | -0.49 |
| TM4-TM11a | HD | -0.89 | TM1b-TM10b | HA | -0.62 | EL4a-TM11a | HD | -0.49 |
| TM1b-TM11a | HD | -0.89 | TM1b-TM12 | HA | -0.61 | **TM5-TM11a** | **HD** | **-0.47** |
| TM2b-TM11a | HD | -0.88 | TM1b-**TM6b** | HA | -0.61 | TM1b-TM10b | HA | -0.46 |
| | | | TM1a-TM6a | HA | -0.61 | **TM8-TM11a** | **HD** | **-0.45** |
| | | | **TM6a-TM11a** | **HA** | **-0.61** | | | |
| | | | **TM5-TM11a** | **HD** | **-0.60** | | | |
| common with PC1 negative pairs | | | | | **7/13** | | | **4/11** |
| total common | | | | | **28/40** | | | **17/40** |

"HD" is the center-of-mass distance between two segments; "HA" is the helix angle between two helical segments. The pairs in bold font are the common ones between Na1/Na2 enthalpy and $\gamma_1$(t). The TMs 1, 6, and 10 are colored in blue, red, and green respectively, with their extracellular and intracellular segments in colored font and shade, respectively.

**Table S3.** Ion selectivity of $Na^+/K^+$ and $Na^+/Li^+$ for the Na1 site at various conformational states.

| ΔG (kcal/mol) | Bulk | Occluded | F1 | F2 | F3 | F4 | F5 | F6 | F7 | F8 |
|---|---|---|---|---|---|---|---|---|---|---|
| $\Delta G_{Na+->K+}$ | 18.49 ±0.08 | - | 20.24 ±0.35 | 22.51 ±0.33 | 21.00 ±0.28 | 22.02 ±0.63 | 21.56 ±0.23 | 20.85 ±0.54 | 21.38 ±0.69 | 21.72 ±0.29 |
| $\Delta G_{K+->Na+}$ | -18.49 ±0.12 | - | -20.20 ±0.49 | -22.20 ±0.33 | -20.98 ±0.36 | -21.49 ±0.36 | -21.55 ±0.36 | -20.39 ±0.29 | -21.36 ±0.52 | -21.22 ±0.42 |
| average $\Delta G_{Na+->K+}$ | 18.49 ±0.14 | 21.90* | 20.22 ±0.60 | 22.36 ±0.47 | 20.99 ±0.46 | 21.76 ±0.73 | 21.56 ±0.43 | 20.62 ±0.61 | 21.37 ±0.86 | 21.47 ±0.51 |
| $\Delta\Delta G_{Na+->K+}$ | - | **3.41*** | **1.7 ±0.6** | **3.9 ±0.5** | **2.5 ±0.5** | **3.3 ±0.7** | **3.1 ±0.5** | **2.1 ±0.6** | **2.9 ±0.9** | **3.0 ±0.5** |
| $\Delta G_{Na+->Li+}$ | -22.84 ±0.30 | - | -22.20 ±0.22 | -23.40 ±0.23 | -23.72 ±0.28 | -23.05 ±0.35 | -22.19 ±0.20 | -23.06 ±0.47 | -24.08 ±0.17 | -23.64 ±0.17 |
| $\Delta G_{Li+->Na+}$ | 22.83 ±0.28 | - | 22.07 ±0.13 | 23.73 ±0.23 | 23.34 ±0.26 | 23.02 ±0.24 | 22.43 ±0.16 | 22.89 ±0.25 | 24.16 ±0.20 | 23.71 ±0.16 |
| average $\Delta G_{Na+->Li+}$ | -22.84 ±0.41 | -22.8* | -22.14 ±0.26 | -23.57 ±0.33 | -23.53 ±0.38 | -23.04 ±0.42 | -22.31 ±0.26 | -22.98 ±0.53 | -24.12 ±0.26 | -23.68 ±0.23 |
| $\Delta\Delta G_{Na+->Li+}$ | - | **0.04*** | **0.7 ±0.5** | **-0.7 ±0.5** | **-0.7 ±0.6** | **-0.2 ±0.6** | **0.5 ±0.5** | **-0.1 ±0.7** | **-1.3 ±0.5** | **-0.8 ±0.5** |

*The selectivities for the occluded state of LeuT with substrate and both ions bound are from ref. (2). The mean ± standard deviation for $\Delta G_{Na+->K+}$, $\Delta G_{K+->Na+}$, $\Delta G_{Na+->Li+}$, and $\Delta G_{Li+->Na+}$ are computed by blocking the last 180 ps of the 200 ps data of each FEP window to 16 blocks. The number of blocks (16) is determined so that the standard error of the mean is no longer increasing as the number of blocks increases from 2 to 4, 8, 16, 32, and 64 (7). The standard deviations (σ) for "average $\Delta G_{Na+->K+}$" and "average $\Delta G_{Na+->Li+}$" are computed as $\sigma_{average\_\Delta G_{Na+->K+}} = \sqrt{\sigma^2_{\Delta G_{Na+->K+}} + \sigma^2_{\Delta G_{K+->Na+}}}$ and $\sigma_{average\_\Delta G_{Na+->Li+}} = \sqrt{\sigma^2_{\Delta G_{Na+->Li+}} + \sigma^2_{\Delta G_{LiK+->Na+}}}$ respectively.

**Movies S1, S2, and S3.** The movies show linear interpolations between negative and positive extremes of deformations along PC1 of MD1 (*S1*), PC1 of MD2 (*S2*), and PC3 of MD1 (*S3*) from their average structures (deformations were limited to RMSD of 0.6 Å from the average structure). The protein is oriented in the same perspective as in Fig. 2 *A*. To compare the motilities near the Na1 site (see text), the TM1b and EL4a in movies S1 and S3 are rendered transparently, and the Cα atoms of Asn27, Asn286, and Glu290 are shown as blue, green, and red spheres, respectively.

**References**


1. Roux, B., S. Berneche, B. Egwolf, B. Lev, S. Y. Noskov, C. N. Rowley, and H. Yu. 2011. Ion selectivity in channels and transporters. *J Gen Physiol* 137:415-426.
2. Caplan, D. A., J. O. Subbotina, and S. Y. Noskov. 2008. Molecular mechanism of ion-ion and ion-substrate coupling in the Na+-dependent leucine transporter LeuT. *Biophys J* 95:4613-4621.
3. Brooks, B. R., C. L. Brooks, 3rd, A. D. Mackerell, Jr., L. Nilsson, R. J. Petrella, B. Roux, Y. Won, G. Archontis, C. Bartels, S. Boresch, A. Caflisch, L. Caves, Q. Cui, A. R. Dinner, M. Feig, S. Fischer, J. Gao, M. Hodoscek, W. Im, K. Kuczera, T. Lazaridis, J. Ma, V. Ovchinnikov, E. Paci, R. W. Pastor, C. B. Post, J. Z. Pu, M. Schaefer, B. Tidor, R. M. Venable, H. L. Woodcock, X. Wu, W. Yang, D. M. York, and M. Karplus. 2009. CHARMM: the biomolecular simulation program. *J Comput Chem* 30:1545-1614.
4. MacKerell, A. D., Jr., M. Feig, and C. L. Brooks, 3rd. 2004. Improved treatment of the protein backbone in empirical force fields. *J Am Chem Soc* 126:698-699.
5. Essmann, U., L. Perera, M. L. Berkowitz, T. Darden, H. Lee, and L. G. Pedersen. 1995. A smooth particle mesh Ewald method. *J Chem Phys* 103:8577-8593.
6. Souaille, M., and B. Roux. 2001. Extension to the weighted histogram analysis method: combining umbrella sampling with free energy calculations. *Computer Physics Communications* 135:40-57.
7. Rapaport, D. C. 2004. The art of molecular dynamics simulation. Cambridge University Press, Cambridge, UK ; New York, NY.